



Research article

Nickel-tolerant zeolite/boron catalysts: Comparing the performances in cracking of light and heavy hydrocarbon model feedstocks

D.E. Adanenche ^{a,b,*}, A.Y. Atta ^a, A. Aliyu ^a, B.J. El-Yakubu ^a^a Department of Chemical Engineering, Ahmadu Bello University, P.M.B 1045, Zaria, Nigeria^b Research and Development Centre, Dangote Petroleum Refinery and Petrochemicals, FZE, Union Marble House, Ikoyi, Lagos, Nigeria

ARTICLE INFO

Keywords:
 Zeolite-Y
 RFCC catalysts
 Nickel
 Deactivation
 Boron
 Passivation

ABSTRACT

The deactivation of zeolite catalysts by nickel deposition during catalytic cracking of nickel-contaminated feedstocks is a significant issue, especially in Residue Fluid Catalytic Cracking (RFCC) processes. This study explores the efficacy of boron modification in mitigating nickel-induced deactivation across three zeolite types (Y-5.1, USY-5.2 and VUSY-12) with variable silica-to-alumina ratios. Nickel was introduced at 30 wt% concentration, while boron loadings ranged from 1 to 10 wt%. The boron-modified zeolites showed a recovery in crystallinity, with increases from 43 % to 93 % at 10 wt% boron. Pyridine-FTIR demonstrated that the introduction of boron enhanced the Bronsted acidity of the nickel-deactivated zeolites. Hydrogen Temperature Programmed Reduction (H_2 -TPR) showed a shift in NiO reduction temperatures from 450–500 °C to 600–700°C upon boron addition, indicating the formation of stronger acid sites. The catalytic performance tests showed that addition of boron effectively suppressed the formation of hydrogen and methane during the catalytic cracking of n-heptane and 1,3,5-triisopropylbenzene (TIPB), demonstrating its effectiveness in mitigating the adverse effects of nickel contamination. Boron modification led to a reduction in hydrogen yield by 30 % for Y-5.1, 56 % for USY-5.2, and 57 % for VUSY-12 during n-heptane cracking. For TIPB cracking, the corresponding reductions in hydrogen production were 22 %, 56 %, and 45 % for Y-5.1, USY-5.2 and VUSY-12, respectively. The level of the enhancement depends on zeolite types and silica-to-alumina ratios. These results suggest that boron enhances the structural stability of zeolite catalysts and mitigates the dehydrogenation effects of nickel, promoting improved performance in RFCC applications.

1. Introduction

The recent shift towards catalytic conversion of heavy crude oil, petroleum residues, and bio-based feedstocks has prompted the development of the residue fluid catalytic cracking (RFCC) process to address the limitations of traditional fluid catalytic cracking (FCC). While conventional FCC relies majorly on the feed from the bottom of the vacuum distillation unit, RFCC directly processes the heavy and contaminated residues from the crude distillation unit into lighter and more valued petroleum products like olefins, cracked gasoline, Light Cycle Oil (LCO), and Heavy Cycle Oil (HCO).

Indeed, implementing RFCC eliminates the need to establish and operate a separate vacuum distillation unit, thereby reducing costs. However, processing the dense and contaminated residues from the atmospheric distillation unit, as well as biomass feedstocks, poses numerous challenges owing to the presence of heteroatom contaminants

such as V, Ni, Na, Fe and high Conradson Carbon Residues (CCR). Among these, Ni is particularly detrimental as it catalyses side reactions, for example, dehydrogenation and excessive coke formation, thereby deactivating the RFCC catalyst.

Nickel compounds, such as porphyrins and naphthenates, have the potential to accumulate on the cracking catalysts during the cracking process. Within the regenerator, these compounds undergo oxidation, yielding NiO as one of the resultant products. NiO undergoes reduction to its elemental form, nickel (Ni^0), upon entry into the reactor riser. This elemental nickel serves as an active dehydrogenation site, facilitating the generation of surplus hydrogen and coke, consequently limiting selectivity to the desired product [1–3]. Moreover, the deposition of nickel oxide and metallic nickel can block pores and reduce the accessibility of active sites, leading to a loss of crystallinity.

In our recent article [4], we provided a detailed investigation into the effects of nickel deactivation on various zeolites (Y-5.1, USY-5.2 and

* Corresponding author at: Research and Development Centre, Dangote Petroleum Refinery and Petrochemicals, FZE, Union Marble House, Ikoyi, Lagos, Nigeria.
 E-mail address: daniel.adanenche@dangoteprojects.com (D.E. Adanenche).

VUSY-12), examining their crystallinity, surface area, pore structure, morphology, acidity, and catalytic performance under varying nickel loadings. The study revealed that higher nickel concentrations (20–30 wt%) led to the detection of nickel oxide (NiO) phases, reduced crystallinity, and potential structural degradation. Nitrogen adsorption-desorption showed mesoporous characteristics, with VUSY-12 maintaining better pore accessibility at low Ni loadings due to its hierarchical structure but experiencing significant pore blockage at 30 wt% Ni. Morphological analyses indicated uniform zeolite particles at 0 wt% Ni, transitioning to NiO-induced agglomeration at higher Ni loadings. NH₃-TPD revealed diminished acid site strength and quantity with increased Ni, particularly in VUSY-12, impacting catalytic efficiency by favouring dehydrogenation over hydrocarbon cracking. Catalytic cracking tests with n-Heptane confirmed shifts in product distribution, favouring light alkanes and olefins alongside increase in the yield of hydrogen and methane as Ni loading increased, with Y-5.1 showing the best catalytic performance. The work underscored the detrimental impact of nickel on zeolite structure and functionality, highlighting the need for strategies to mitigate Ni-induced degradation in hydrocarbon cracking applications.

There have been efforts to mitigate the negative impacts of nickel in zeolites-Y based catalysts used for the catalytic cracking of hydrocarbons. BASF, a leading manufacturer of cracking catalysts, carried out a comparative analysis of catalysts with nickel passivation versus those without. Their findings showed that the application of antimony for passivation increased NO_x production by 20 % [5]. The increase was as a result of the presence of antimony within the cracking environment, which may change the conversion pathways of nitrogen compounds, thereby enabling the production of NO_x precursors such as hydrogen cyanide (HCN) or ammonia (NH₃). Inside the regenerator, these precursors are oxidized to NO_x instead of being completely reduced to nitrogen gas (N₂). Moreover, it was observed that antimony presents considerable handling hazards and can contribute to the fouling of processing equipment [6]. Substitute materials, such as silica-doped aluminas, lanthanum, and phosphorus have also been used by refiners to offset the detrimental effects of nickel [6–8]. For example, research by Yue *et al.* [7] observed the efficacy of mesoporous silica-doped aluminas in nickel passivation. Nonetheless, it was determined that alumina's effectiveness is reduced under RFCC conditions due to its high peripheral deposition index, which limits its mobility within the system [9].

New studies have underscored the potential of boron as an effective passivator, due to its outstanding capacity to decrease dehydrogenation and prevent coke formation [10–13]. For example, density functional theory (DFT) calculations were used to examine the influence of boron on the surface of cobalt, indicating that boron mimics carbon adsorption by occupying octahedral sites in the first subsurface layer of the metal. The selective occupation impedes the diffusion of carbon into the metal lattice, thereby reducing the formation of both hydrogen and carbon species [10]. Over the past few decades, the effects of boron on Al₂O₃--supported nickel catalysts have been extensively studied. For example, the modification of a 15 % Ni/Al₂O₃ catalyst with 1 % boron resulted in an 80 % reduction in dehydrogenation and carbon deposition during methane steam reforming [12]. In another investigation, a boron-modified nickel catalyst was utilized for the Fischer-Tropsch synthesis, where boron addition reduced the rate of catalyst deactivation by a factor of six without compromising catalytic activity [11]. More recently, it has been shown that incorporating boron into Ni/Al₂O₃ catalysts diminishes dehydrogenation and regulates the size of nickel particles [13].

The aforementioned studies indicate that boron can effectively inhibit hydrogen and carbon formation on catalyst surfaces. However, no comprehensive study has explored the synergistic effects of boron and nickel on high-surface-area mesoporous zeolites across a wide range of concentrations, particularly for the catalytic cracking of light and heavy petroleum feedstocks. n-Heptane and 1,3,5-triisopropylbenzene (TIPB) were chosen as model feedstocks for their distinct structural

and chemical traits, offering complementary insights into catalytic performance. n-Heptane, a linear alkane, represents a class of light hydrocarbons prone to cracking and dehydrogenation, making it an ideal candidate for evaluating the acid site strength and distribution in zeolites. TIPB, an aromatic compound with bulky substituents, serves as a representative heavy feedstock that challenges the accessibility and efficacy of active sites within the catalyst's porous architecture. Together, these feedstocks enable a comprehensive assessment of catalytic activity under varying reaction conditions and feed complexities, reflecting the practical diversity encountered in RFCC processes. Further investigations are needed to provide additional insight into boron's role in mitigating nickel's deleterious effects. Therefore, this work aims to conduct a comparative analysis of the performance of varying boron loadings on three different nickel-deactivated zeolites: zeolite-Y (Y-5.1), ultra-stable Y (USY-5.2) and very-ultra-stable Y (VUSY-12) in the cracking of n-Heptane and 1,3,5-Triisopropylbenzene. The principal focus of this research is to explore the physicochemical interactions amongst boron, nickel, and the zeolite framework. Hydrogen temperature-programmed reduction (H₂-TPR), X-ray diffraction (XRD), and pyridine Fourier-transform infrared spectroscopy (Py-FTIR) are the characterisation techniques that will be used to study the physicochemical changes in the zeolites caused by the deposition of boron and nickel. Moreover, the catalytic activities of the modified zeolites will be assessed using both light and heavy hydrocarbon feedstocks.

2. Experimental

2.1. Zeolite preparation

The impact of boron on the nickel-induced deactivation of zeolite catalysts was studied using three separate zeolite substrates distinguished by their silica to alumina ratios: zeolite-Y, ultra-stable-Y (USY), and very-ultra-stable-Y (VUSY). The deposition of nickel onto each zeolite was done at a concentration of 30 wt% using the procedure established by Adanenche *et al.* [4]. Precisely, the zeolite samples underwent calcination at 650°C for 5 h to remove ammonia and change the ammonium form of the zeolites into their hydrogen form. Afterward, nickel was added to the zeolites through the wet impregnation process. The process involved preparing a 30 wt% nickel solution by dissolving nickel naphthenate (C₂₂H₁₄NiO₄, containing approximately 10 % nickel) in cyclohexane (C₆H₁₂, of analytical reagent grade). A similar procedure was used for the boron impregnation of the resulting Ni/zeolites, utilising boric acid as the boron source. Boron was deposited onto the Ni/zeolites at concentrations of 1, 3, 7, and 10 wt% by dissolving the suitable amount of boric acid in water. The zeolites were slowly added to the solutions while continuously stirring at a rate of 3 rpm, maintaining a temperature of 90°C until all the solvent evaporated, resulting in a viscous substance. The resultant viscous materials were then dried in an oven at 100°C for 24 h and calcined in a muffle furnace at 650°C for 5 h.

2.2. Zeolite characterisation

The procedure for the X-ray diffraction (XRD) analysis was adapted from previous studies [4]. Precisely, a Rigaku MiniFlex 6 G system was used with CuK α radiation (1.540593 Å) as the X-ray source. 2 g of powdered samples were compressed into sample holders to ensure uniformity. It was then scanned across a 2θ range of 2–70° with a 0.02° step size, and analysed using the STUDIO SMART LAB II software alongside ICDD PDF-4 databases.

The ATR-FTIR analysis was conducted following the methodology outlined in a previous article [4]. Spectra were collected using a Cary 630 Agilent FTIR spectrometer within the 650–4000 cm⁻¹ range at a resolution of 8 cm⁻¹. For analysis, powdered samples were pressed onto the ATR crystal to ensure optimal contact. For pyridine (Py)-FTIR analysis, samples were degassed at 250°C for 2 h, exposed to pyridine

under vacuum for 3 h, and subsequently analysed via ATR-FTIR.

Hydrogen-Temperature Programmed Reduction (H_2 -TPR) technique was used to assess the hydrogen reducibility of the zeolite samples on a Micromeritics Auto Chem 2920 apparatus. 50 mg of the sample was subjected to pre-treatment with argon gas at a flow rate of 32 mL per minute for one hour at 500°C, followed by cooling to 100°C in the same gas atmosphere. Afterward, the gas flow was changed to a mixture of 10 % hydrogen and argon at a rate of 50 cm³ at standard temperature and pressure (STP) per minute. The H_2 -TPR experiment was carried out within a temperature range of 100–800°C, with a ramping rate of 10°C per minute. Thermal conductivity detector was used to monitor the hydrogen consumption during the H_2 -TPR process.

2.3. Zeolite testing

The procedure used for catalytic cracking was adapted from previous research [4]. Fixed-bed micro-activity test (MAT) unit was used to conduct the reactions involving n-Heptane and 1,3,5-triisopropylbenzene under atmospheric pressure, employing nitrogen as a diluent. Preceding the catalytic tests, the reactor bed was conditioned under a nitrogen flow of 400 mL/min at 550°C for two hours. The same conditions (550°C, atmospheric pressure, 1-h residence time) was used to perform thermal cracking to establish a baseline for catalytic performance. The experiment involving catalytic cracking utilised 0.5 g of catalyst mixed with 1 g of glass beads and packed into the reactor, with n-Heptane and 1,3,5-triisopropylbenzene introduced at a rate of 4 mL/min by a peristaltic pump, while maintaining a nitrogen flow of 400 mL/min. The reactor outlet was directed into a condenser for product collection. The resulting condensed liquid products were analysed using an Agilent 7890B gas chromatograph coupled with an Agilent 5977 A mass selective detector (MSD). The system was equipped with an DB-624 capillary column (30 m × 0.25 mm ID × 0.25 μm film thickness, Agilent Technologies). The GC was operated in splitless injection mode with helium as the carrier gas at a flow rate of 1.0 mL/min. The injection volume was 1 μL using an Agilent G4513A autosampler, and the inlet temperature was set at 250°C. The column oven temperature program was as follows: Initial temperature of 40°C, held for 2 minutes, first ramp of 10 °C/min to 150°C, held for 3 minutes, second ramp of 20 °C/min to 280°C, held for 5 minutes. The total runtime for each sample was 28 minutes. The mass spectrometer was operated in electron ionization (EI) mode at 70 eV. The ion source temperature was set to 230°C, with the quadrupole temperature maintained at 150°C. Data were collected in full scan mode over a mass range of 40–550 m/z. A solvent delay of 3 minutes was applied to prevent contamination of the mass spectrometer by the solvent. Uncondensed gases were channelled to a Gas Board gas analyser to monitor hydrogen (H_2) and methane (CH_4).

3. Results and discussion

3.1. XRD of the nickel and boron-modified zeolites-Y

Three nickel-deactivated zeolites, Y-5.1, USY-5.2, and VUSY-12 containing 30 wt% nickel each were subjected to boron impregnation to assess the efficacy of boron in mitigating the detrimental effects associated with nickel deactivation. The X-ray diffraction (XRD) patterns of the boron-modified zeolites (Ni/B-zeolites) are presented in Fig. 1. Notably, the XRD analysis revealed that the boron-modified zeolites retained the characteristic diffraction peaks of Y-zeolites, indicating the preservation of the crystalline framework post-boron modification, as observed in previous studies [14]. An important observation from the XRD data is the noticeable increase in diffraction intensities of the boron-modified zeolites in relation to their nickel-deactivated counterparts. The increase in intensity suggests an increase in crystallinity attributable to the incorporation of boron, which is quantitatively supported by the calculated percent relative

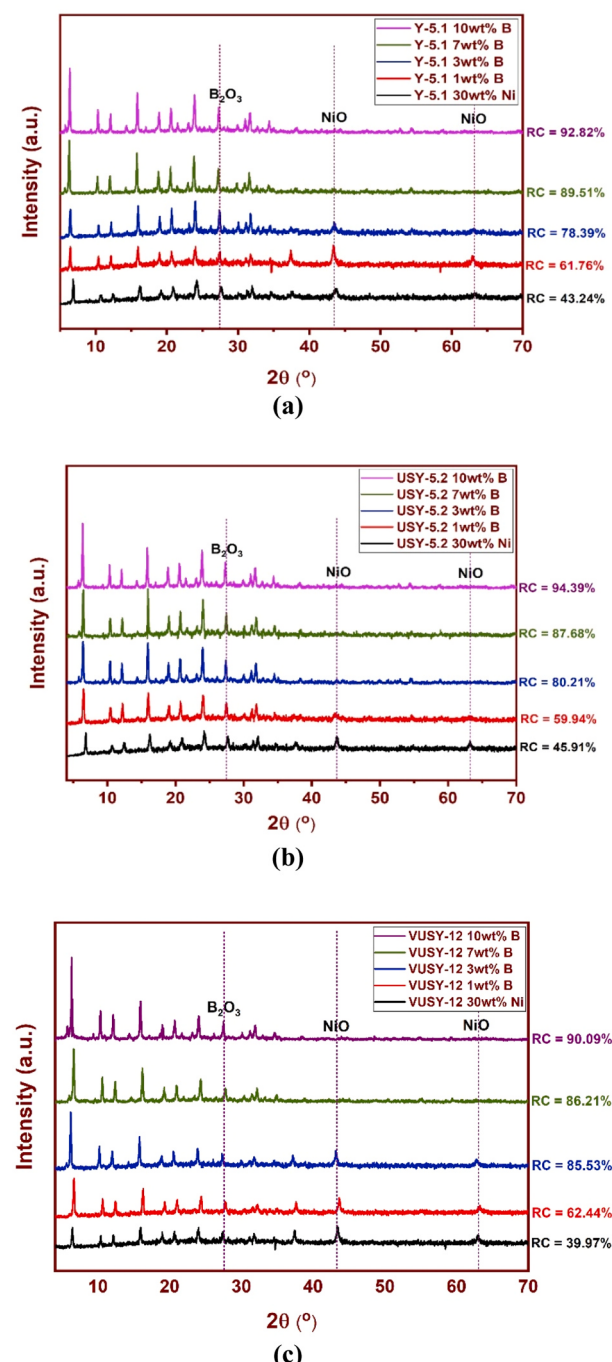


Fig. 1. XRD patterns of boron-modified zeolites (a) Y-5.1, (b) USY-5.2, and (c) VUSY-12 at varying boron concentrations.

crystallinities (RC). For example, as presented in Fig. 1a, the RC of the Y-5.1 sample increased from 43 % to a remarkable 93 % as boron concentrations increased. The same trend was noted for the USY-5.2 and VUSY-12 samples, further supporting the notion that boron modification positively impacts the structural integrity of the zeolite framework. The observed improvement in crystallinity with increase in boron concentrations may be connected with the formation of boron oxide (B_2O_3) species [15], as shown by the appearance of diffraction peaks corresponding to B_2O_3 at a 2θ Bragg's angle of 28°, as presented in Fig. 1. The intensity of these B_2O_3 diffraction peaks correlates positively with boron concentration, suggesting that the presence of boron stabilises the zeolite structure and

may also facilitate the formation of additional crystalline phases.

Moreover, the observed improvement in crystallinity with increase in boron concentrations may also be attributed to the formation of nickel borates (NiB_2O_4) as reported in previous studies [16]. This explains the preserved crystalline framework post-boron modification as earlier observed. These findings underscore the potential of boron as a modifying agent to mitigate the adverse effects of nickel deactivation in zeolite catalysts, thereby enhancing their performance in catalytic applications.

3.2. Pyridine-FTIR of boron-modified zeolites-Y

The FTIR spectra of Pyridine (Py)-adsorbed zeolites are shown in Fig. 2. The bands at 1452 and 1543 cm^{-1} are assigned to the Lewis and Brønsted acid sites, respectively, while the band at 1490 cm^{-1} indicates Brønsted plus Lewis acid sites [17,18]. Because the Brønsted acid site is responsible for hydrogen transfer reactions and due to its dominant role in cracking reactions [19], the bands at 1543 cm^{-1} were carefully compared. The FTIR spectra showed that the intensities of the bands increased with an increase in boron concentration. This suggests that modifying the nickel-deactivated zeolites with boron tends to increase the quantity of the Brønsted acid sites as depicted by the mechanism in Eq. 6. This observation may be because when boron is introduced into the zeolite, it substitutes the aluminum species in the zeolite framework. This boron substitution can alter the electronic properties of the zeolite in the sense that boron is less electronegative than aluminium, which means that boron-containing sites may have a higher proton density than aluminium-containing sites. This increased proton density can lead to stronger proton donating ability, enhancing Brønsted acidity and improving catalytic activity [20,21].

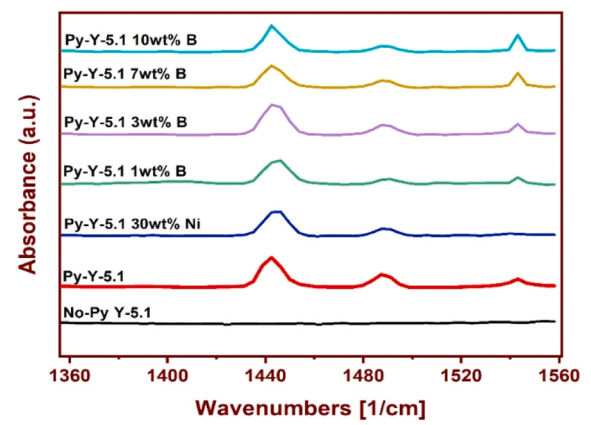
Moreover, due to the electronegativity of boron and its ability to form strong bonds with oxygen, boron can stabilize the proton sites associated with Brønsted acidity. The boron-oxygen bond within the framework is less polarizable than the silicon-oxygen bond, making the protons more localized and easier to access for catalytic reactions [22]. This leads to stronger and more stable Brønsted acid sites, which can enhance catalytic activity, particularly for reactions that rely on hydrogen transfer mechanisms, such as cracking.

Table 1 further confirmed the improvement in Brønsted acidity with increased boron concentration. For example, it could be observed that before nickel deactivation, Y-5.1 possessed $1768\text{ }\mu\text{mol/g}$ of Brønsted acidity, which drastically reduced to $1097\text{ }\mu\text{mol/g}$ upon deactivation with 30 wt\% Ni . Modification with $1, 3, 7$ and 10 wt\% boron improved the Brønsted acidity with increased boron concentration. However, only 10 wt\% B restored the Brønsted acidity to $1320\text{ }\mu\text{mol/g}$ above the nickel-deactivated value for Y-5.1. The same trend could be observed for USY-5.2, except for every increment in boron concentration, the quantity of Brønsted acid sites improved above the nickel-deactivated USY-5.2. Interestingly, VUSY-12 exhibited a different behaviour. For all boron concentrations, the Brønsted acidity is even better than the parent zeolite before deactivation with 30 wt\% Ni . It may be due to the relatively high mesoporosity of that zeolite, facilitating easy migration of the boron into the pores to substitute the aluminium species in the zeolite framework.

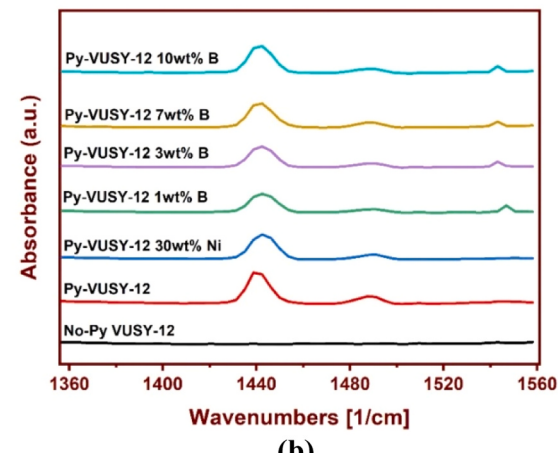
The number of acid sites as presented in Table 1 was determined using pyridine-FTIR spectroscopy. Pyridine was adsorbed onto the zeolite samples, and the intensities of the characteristic bands at 1452 cm^{-1} (Lewis acid sites) and 1543 cm^{-1} (Brønsted acid sites) were measured. The amount of pyridine adsorbed was quantified using calibration curves, and the acid site concentrations were calculated based on the integrated areas of these bands. The total acid sites were obtained by summing the Lewis and Brønsted acid sites. This method is well-established in the literature for quantifying acid sites in zeolites.

3.3. H_2 -TPR of boron-modified zeolites-Y

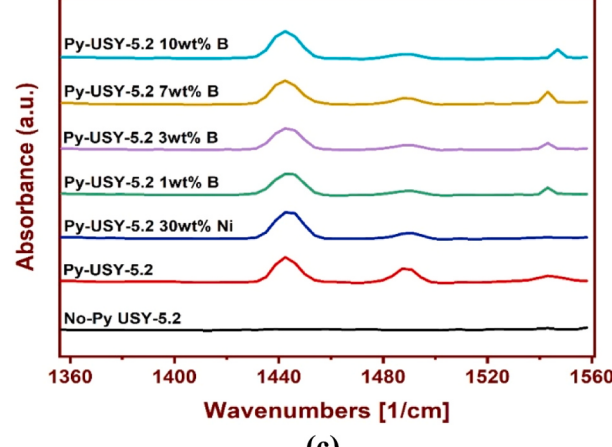
The results of the hydrogen temperature programmed reduction (H_2 -



(a)



(b)



(c)

Fig. 2. Pyridine (Py)-FTIR of: (a) Y-5.1, (b) USY-5.2, and (c) VUSY-12 at varying boron concentrations.

TPR) analysis for the nickel-supported zeolites (Ni/zeolites) and boron-modified nickel-supported zeolites (Ni/B-zeolites) are presented in Fig. 3. The reduction of nickel oxide (NiO) in the Ni/zeolite samples is characterized by distinct peaks observed within the temperature range of $450\text{--}500^\circ\text{C}$. This observation indicates the thermal reduction of NiO to metallic nickel under the applied hydrogen atmosphere. In contrast, the Ni/B-zeolite samples exhibit a notable shift in the reduction temperatures of NiO to higher values, with peaks occurring at elevated and

Table 1

Quantity of Lewis, Bronsted and total acid sites of Y-5.1, USY-5.2, and VUSY-12 at 30 wt% Ni and varying boron concentrations.

Samples	mmol/g		mmol/g
	Lewis	Bronsted	
Py-Y-5.1	2493	1768	4261
Py-Y-5.1 30 wt% Ni	1940	1097	3037
Py-Y-5.1 1 wt% B	1631	742	2373
Py-Y-5.1 3 wt% B	1649	879	2328
Py-Y-5.1 7 wt% B	1224	910	2135
Py-Y-5.1 10 wt% B	1293	1320	2613
Py-USY-5.2	1955	1733	3688
Py-USY-5.2 30 wt% Ni	2104	715	2819
Py-USY-5.2 1 wt% B	2219	901	3120
Py-USY-5.2 3 wt% B	1287	940	2228
Py-USY-5.2 7 wt% B	1415	978	2393
Py-USY-5.2 10 wt% B	1962	1002	2965
Py-VUSY-12	2613	886	3499
Py-VUSY-12 30 wt% Ni	1949	646	2596
Py-VUSY-12 1 wt% B	2038	1034	3072
Py-VUSY-12 3 wt% B	1364	1036	2401
Py-VUSY-12 7 wt% B	1460	1037	2497
Py-VUSY-12 10 wt% B	2041	1041	3082

more stable temperatures as the boron concentration increased. Precisely, the reduction temperatures for NiO in the presence of boron were found to range from 600 to 700°C at boron loadings of 7 and 10 wt%. The observed reduction temperature may be due to the formation of highly stable nickel borate species, predominantly NiB_2O_4 , which significantly impedes the reduction of NiO. The exceptional passivation effect of boron-modified zeolites on nickel species is a key factor contributing to this stabilisation, as buttressed by the findings of Yuan *et al.* [14]. The significances of these results are particularly important in the context of the Residual Fluid Catalytic Cracking (RFCC) process. This is because, observed reduction temperatures for the boron-modified zeolites exceed the operational temperatures typically used in RFCC units, suggesting that the reduction of NiO will be considerably impeded when processing feedstocks with nickel concentrations as high as 30 wt %. This finding suggests that the incorporation of boron into nickel-deactivated zeolite matrices is an effective strategy to alleviate the reduction of nickel species, thereby improving the stability and longevity of the catalyst in RFCC applications.

3.4. Catalytic performances of the nickel and boron-modified zeolites

The product distribution resulting from the catalytic cracking of n-heptane over the boron-modified catalysts is depicted in Fig. 4 with the detailed individual compounds presented in Tables A 1, A 2, and A 3 of the [supplementary materials](#). It is evident that there was a negligible change in the yield of C₅–C₆ alkanes and olefins as boron concentration increased. However, increasing boron concentration was observed with a concomitant rise in the abundance of heavier hydrocarbons (C₇₊). This phenomenon may be attributed to the decreased yield of hydrogen gas, leading to the formation of heavier hydrocarbon products.

The catalytic influence of boron is further reflected in the distribution patterns of hydrogen and methane. A progressive decline in hydrogen and methane production was noted as boron concentration increased. This finding highlights boron's capability to passivate nickel's dehydrogenation activity, thereby reducing gaseous product formation and preserving the yield of light alkanes and olefins, which are crucial constituents of gasoline blends. Additionally, at a constant boron concentration across the three zeolites, the reduction in light alkanes, olefins, hydrogen, and methane followed the sequence Y-5.1 > USY-5.2 > VUSY-12. This trend correlates with the increasing silica-to-alumina ratios in the aforementioned order, aligning with the distribution of acid sites as elucidated by the NH₃-TPD study reported by Adanenche *et al.* [4]

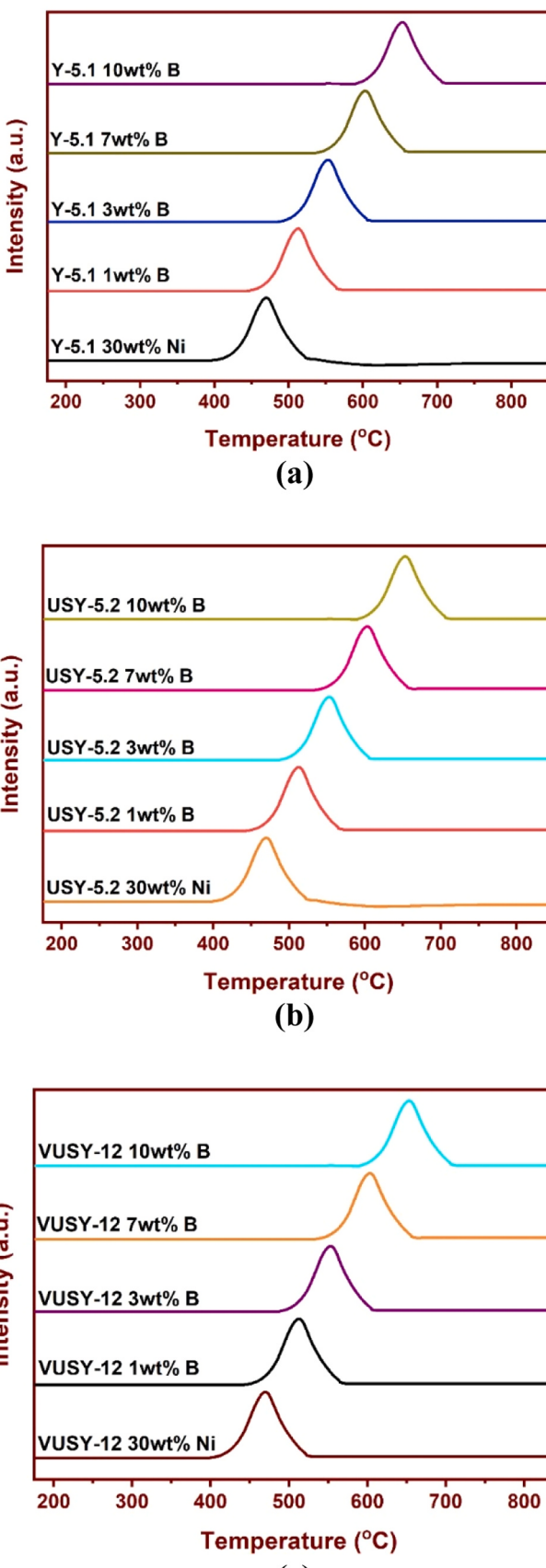


Fig. 3. H₂-TPR of: (a) Y-5.1, (b) USY-5.2, and (c) VUSY-12 at varying boron concentrations.

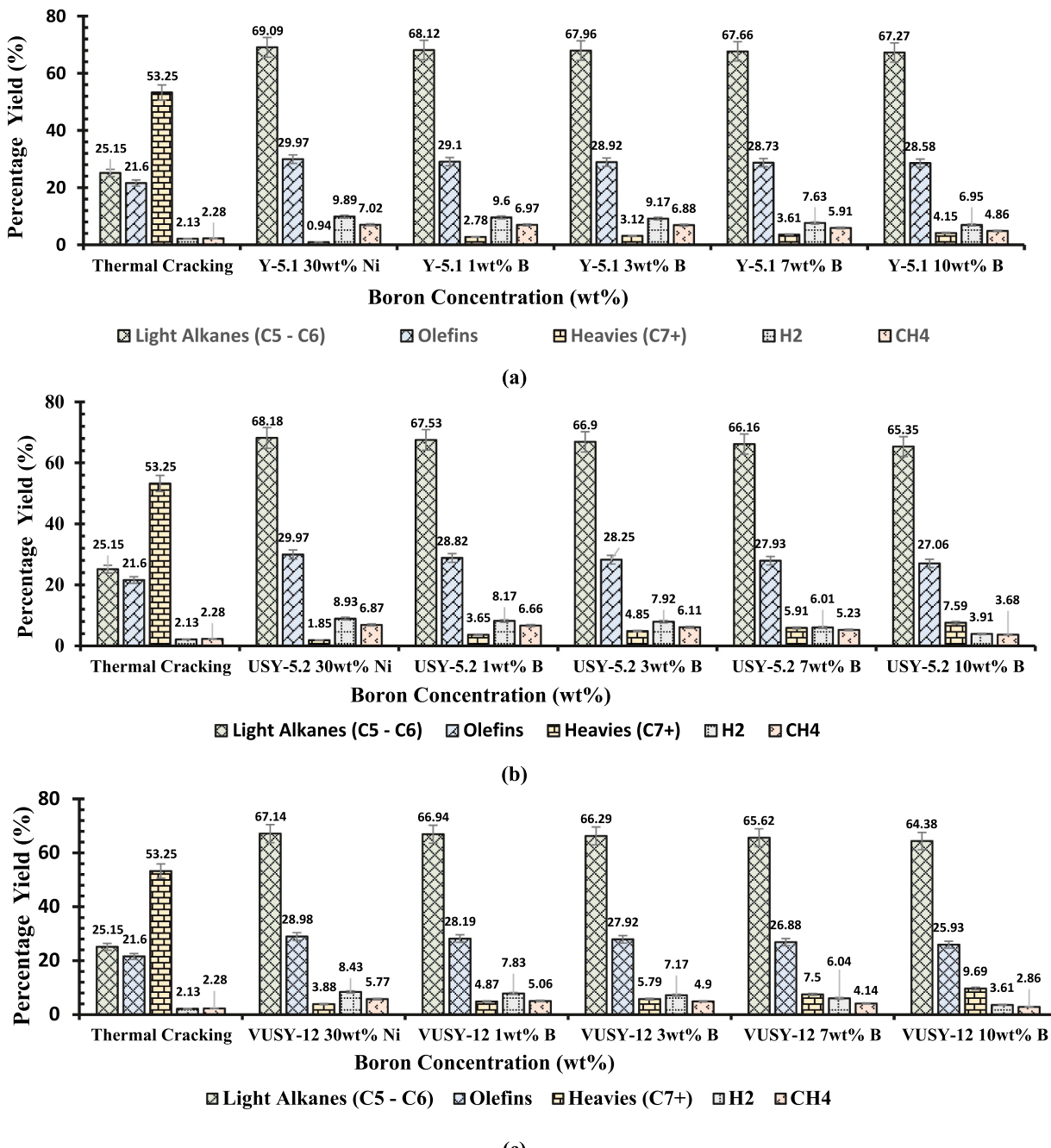


Fig. 4. Products distribution of n-Heptane cracking over (a) Y-5.1, (b) USY-5.2, and (c) VUSY-12 at varying boron concentrations.

3.5. Catalytic performances of the Nickel and boron-modified zeolites on Heavier Feedstock

The catalytic cracking of a heavier model feedstock 1,3,5-Tri-isopropylbenzene (TIPB) was conducted in a fixed-bed reactor to assess the catalytic efficacy of zeolites loaded with 30 wt% nickel and 10 wt% boron. Fig. 5 illustrates the product distribution derived from this cracking process with the detailed individual compounds presented in Tables A 4 of the supplementary materials. Notably, principal products of TIPB cracking include di-isopropyl benzene (DIPB) isomers, isopropyl benzene (IPB), and benzene. As depicted in Fig. 5, the VUSY-12 zeolite yields a higher proportion of DIPB, while the formation of deep cracking products, such as IPB and benzene, is minimal. This contrasts with the performance of Y-5.1 and USY-5.2, where a more significant proportion of deep cracking products is observed relative to VUSY-12. These

findings suggest that the mesoporous structure of VUSY-12 facilitates the production of DIPB, likely due to the contribution of abundant mesopores to the initial cracking of TIPB. Furthermore, the mesopores in VUSY-12 enhance mass transfer efficiency for the bulky TIPB molecules, providing a pathway for initial cracking into intermediate-sized molecules, which can subsequently undergo further cracking within the zeolites' micropores.

The distributions of hydrogen and methane during the cracking of n-heptane and 1,3,5-tri-isopropylbenzene over Y-5.1, USY-5.2, and VUSY-12 zeolites, each containing 30 wt% nickel and 10 wt% boron, are presented in Table 2. Notably, hydrogen and methane production are higher for n-heptane compared to TIPB across all zeolites at identical nickel and boron concentrations. This disparity can be attributed to the tendency of n-heptane to lose hydrogen atoms more readily due to the presence of hydrogen atoms bonded to sp^3 -hybridized carbons.

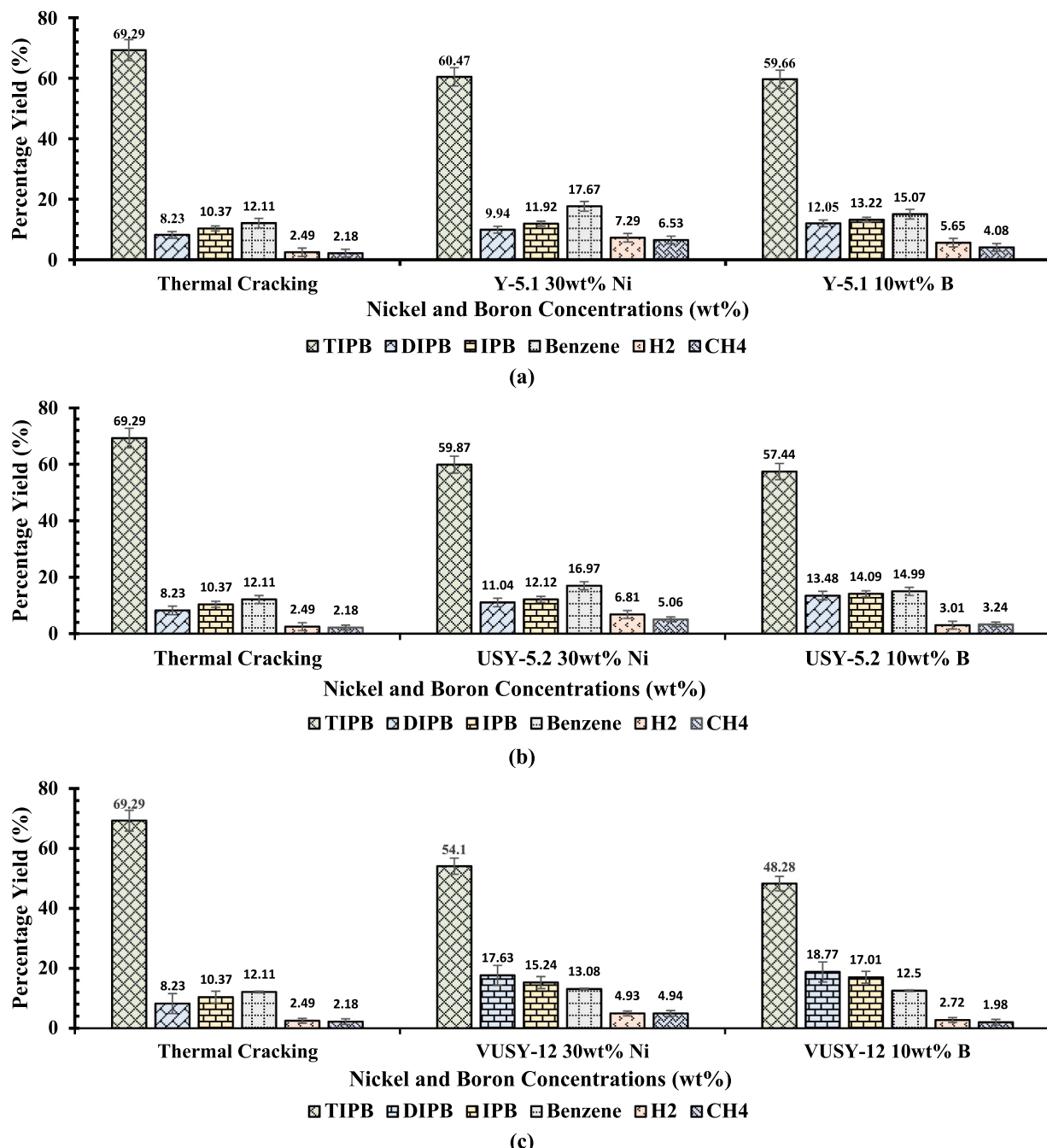


Fig. 5. Product distribution of 1,3,5-Triisopropylbenzene cracking over: (a) Y-5.1, (b) USY-5.2 and (c) VUSY-12 at 30 wt% Ni and 10 wt% boron.

Table 2

Hydrogen and methane distribution of Y-5.1, USY-5.2 and VUSY-12 at 30 wt% Ni and 10 wt% B.

Catalyst	H ₂		CH ₄	
	n-Heptane	1,3,5-TIPB	n-Heptane	1,3,5-TIPB
Y-5.1 30 wt% Ni	9.89	7.29	7.02	6.53
USY-5.2 30 wt% Ni	8.93	6.81	6.87	5.06
VUSY-12 30 wt% Ni	8.43	4.93	5.77	4.94
Y-5.1 10 wt% B	6.95	5.65	4.86	4.08
USY-5.2 10 wt% B	3.91	3.01	3.68	3.24
VUSY-12 10 wt% B	3.61	2.72	2.86	1.98

Conversely, 1,3,5-Tri-isopropylbenzene, with its three isopropyl substituents, is an aromatic compound whose resonance-stabilized aromatic ring confers inherent stability.

The dehydrogenation of aromatic compounds is inherently more difficult than alkanes because it would require breaking the aromatic stability. The isopropyl groups attached to the benzene ring contribute minimally to dehydrogenation because the aromatic ring is already in a stable state and is not significantly altered by such reactions. Consequently, the simpler structure and higher reactivity of n-heptane render it more susceptible to dehydrogenation in the presence of these catalysts compared to TIPB. This rationale elucidates the lower hydrogen and methane production observed during TIPB cracking, as detailed in Table 2.

Furthermore, the incorporation of boron into the zeolite framework resulted in a marked reduction in hydrogen production during the

catalytic cracking of n-heptane and 1,3,5-triisopropylbenzene (TIPB), demonstrating its effectiveness in mitigating the adverse effects of nickel contamination. Specifically, boron modification led to a reduction in hydrogen yield by 30 % for Y-5.1, 56 % for USY-5.2, and 57 % for VUSY-12 during n-heptane cracking. For TIPB cracking, the corresponding reductions in hydrogen production were 22 %, 56 %, and 45 % for Y-5.1, USY-5.2, and VUSY-12, respectively. Similarly, a significant decrease in methane production was observed under the same conditions. Methane yields were reduced by 31 %, 46 %, and 50 % in Y-5.1, USY-5.2, and VUSY-12, respectively, during n-heptane cracking, while for TIPB cracking, methane reductions were 38 %, 36 %, and 60 % for Y-5.1, USY-5.2, and VUSY-12, respectively.

These results underscore the efficacy of boron in passivating the detrimental effects of nickel by significantly suppressing the formation of hydrogen and light hydrocarbon gases, which are typically associated with undesirable secondary reactions. The substantial decrease in hydrogen and methane yields across different zeolite types indicates that boron modification can effectively neutralize nickel-induced dehydrogenation reactions, improving the overall selectivity of the cracking process toward higher-value products.

3.6. Proposed mechanisms of nickel deactivation and boron passivation in cracking of hydrocarbons as investigated in this study

The detailed reaction mechanisms that demonstrate the nickel deactivation and subsequent boron passivation as discussed in this study are outlined as follows:

3.6.1. Nickel deactivation mechanism

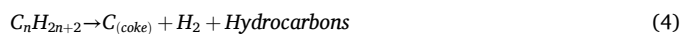
Nickel primarily deactivates zeolite catalysts by facilitating unwanted dehydrogenation and carbon formation reactions. During cracking, nickel is deposited on the catalyst from nickel containing feedstocks in the form of naphthenate. Nickel compounds then oxidise in the regenerator to nickel oxide (NiO) according to Eq. 1:



The nickel oxide formed is then reduced to metallic nickel in the reactor riser according to Eq. 2:



Here, metallic nickel catalyses dehydrogenation, producing surplus hydrogen and carbon species. The following reaction represents this dehydrogenation and coke formation on nickel sites, which competes with the desired cracking reaction:



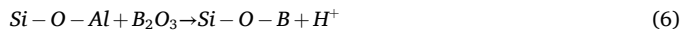
3.6.2. Boron passivation mechanism

To mitigate nickel-induced deactivation, boron is introduced into the zeolite framework. Boron works by forming stable boron compounds with nickel oxide and altering the zeolite's acid site distribution, thus reducing nickel's dehydrogenation activity. The following reaction illustrates this interaction:



This reaction shifts the reduction temperature of NiO , creating more stable nickel-boron oxide complexes like nickel borate (NiB_2O_4), which are less reactive in dehydrogenation, thereby suppressing hydrogen and carbon formation.

The incorporation of boron introduces additional Bronsted acid sites in the zeolite matrix according to the following equation:



These Bronsted acid sites facilitates cracking reactions over dehydrogenation, favouring the production of desired hydrocarbons such as light alkanes and olefins, over hydrogen and methane. This change enhances the cracking efficiency while mitigating undesirable side reactions.

4. Conclusion

This study presents a significant advancement in the understanding of boron-modified zeolite catalysts, specifically addressing the challenge of nickel-induced deactivation in catalytic cracking processes. The physicochemical and catalytic effects of incorporating boron at concentrations ranging from 1 to 10 wt% was examined by employing zeolites of varying silica-to-alumina ratios (Y-5.1, USY-5.2, and VUSY-12) as catalyst substrates. Using n-heptane and 1,3,5-triisopropylbenzene (TIPB) as model feedstocks, the interplay between boron and nickel in mitigating deactivation effects was systematically evaluated. Key findings demonstrate that boron incorporation restored and enhanced the structural and acidic properties of the nickel-deactivated zeolites. Crystallinity recovery reached up to 93 %, and Bronsted acidity improved significantly, as evidenced by pyridine-FTIR. Furthermore, $\text{H}_2\text{-TPR}$ analysis revealed a stabilization of nickel species, with a shift in reduction temperatures, reducing the tendency for undesirable dehydrogenation reactions. Catalytic performance tests validated these findings, showing reductions in hydrogen and methane formation by up to 57 % and 50 %, respectively, depending on the zeolite type and feedstock. Notably, VUSY-12 exhibited superior performance in cracking heavier hydrocarbons due to its hierarchical mesoporous structure. From a broader perspective, this research offers a pathway to enhance RFCC operations by reducing hydrogen formation, which is detrimental to process efficiency and product yields. The study underscores boron's potential as an environmentally friendly and cost-effective passivator, compared to traditional approaches involving antimony or lanthanum. By improving catalyst durability and selectivity, the findings contribute to more sustainable and economically viable refining processes, with implications for reducing waste and lowering operational costs in industries handling nickel-contaminated feedstocks.

5. Limitations of the research

The following limitations were identified during the course of this research. Note that these constraints are not merely supplementary details for future exploration, but rather specific parameters and conditions that should recalibrate the interpretation and significance of the findings in this work.

- i. Most of the sample characterisations and analyses were performed overseas due to non-availability of equipment in our current laboratory.
- ii. The non-condensing gases from Micro-Activity Test (MAT) unit were analysed using a Gas Analyzer, rather than Gas Chromatography.
- iii. Michelle method, rather than more widely used Advanced Cracking Evaluation (ACE) unit was used for catalyst deactivation.

CRediT authorship contribution statement

D.E. Adanenche: Conceptualization, Investigation, Data curation, Writing – original draft, Visualisation, Funding acquisition. **A.Y. Atta:** Writing – review & editing, Supervision. **A. Aliyu:** Visualisation, Writing – review & editing, Supervision. **B.J. El-Yakubu:** Validation, Writing – review & editing, Supervision.

Declaration of Competing Interest

The authors declare that they have no known competing financial interests or personal relationships that could have appeared to influence the work reported in this paper.

Acknowledgements

The authors thank Dangote Petroleum Refinery and Petrochemicals FZE, Nigeria, for the financial support (Grant number: NEFZA/0660).

Appendix A. Supporting information

Supplementary data associated with this article can be found in the online version at [doi:10.1016/j.nxmate.2025.100707](https://doi.org/10.1016/j.nxmate.2025.100707).

References

- [1] W. Letzsch, Fluid catalytic cracking (FCC) in petroleum refining, in: S.A. Treese, P. R. Pujadó, D.S.J. Jones (Eds.), *Handbook of Petroleum Processing*, Springer International Publishing, Cham, 2015, pp. 261–316, https://doi.org/10.1007/978-3-319-14529-7_2.
- [2] U.J. Etim, B. Xu, P. Bai, R. Ullah, F. Subhan, Z. Yan, Role of nickel on vanadium poisoned FCC catalyst: a study of physiochemical properties, *J. Energy Chem.* 25 (2016) 667–676, <https://doi.org/10.1016/j.jechem.2016.04.001>.
- [3] E.T.C. Vogt, B.M. Weckhuysen, Fluid catalytic cracking: recent developments on the grand old lady of zeolite catalysis, *Chem. Soc. Rev.* 44 (2015) 7342–7370, <https://doi.org/10.1039/C5CS00376H>.
- [4] D.E. Adanenche, A.Y. Atta, A. Aliyu, B.J. El-Yakubu, Effects of nickel-deactivations on zeolites-Y of different SiO₂/Al₂O₃ ratios in catalytic cracking of hydrocarbons, *Materials* 7 (2025) 100413, <https://doi.org/10.1016/j.nxmate.2024.100413>.
- [5] BASF, Boron-Based Technology: An Innovative Solution for Resid FCC Unit Performance Improvement, Presentation (2018).
- [6] D.E. Adanenche, A. Aliyu, A.Y. Atta, B.J. El-Yakubu, Residue fluid catalytic cracking: a review on the mitigation strategies of metal poisoning of RFCC catalyst using metal passivators/traps, *Fuel* 343 (2023) 127894, <https://doi.org/10.1016/j.fuel.2023.127894>.
- [7] M.B. Yue, T. Xue, W.Q. Jiao, Y.M. Wang, Performance of mesoporous silica-doped aluminas on nickel passivation, *Mater. Lett.* 91 (2013) 115–117, <https://doi.org/10.1016/j.matlet.2012.09.104>.
- [8] Y. Qi, Q. Liu, Z. Chen, Y. Zhu, Y. Chen, H. Song, B. Dai, L. Zhang, Nickel-passivating element selection in FCC process and mechanistic study on the passivation of nickel by lanthanum and phosphorus, *Chem. Eng. J.* 467 (2023) 143452, <https://doi.org/10.1016/j.cej.2023.143452>.
- [9] C. Senter, M.C. Mastry, A.M. Mannion, R. McGuire, D. Houtz, B. Yilmaz, Quantitative visual characterization of contaminant metals and their mobility in fluid catalytic cracking catalysts, *Catalysts* 9 (2019) 831, <https://doi.org/10.3390/cata9100831>.
- [10] M. Saeys, K.F. Tan, J. Chang, A. Borgna, Improving the stability of cobalt Fischer–Tropsch catalysts by boron promotion, *Ind. Eng. Chem. Res.* 49 (2010) 11098–11100, <https://doi.org/10.1021/ie100523u>.
- [11] K.F. Tan, J. Chang, A. Borgna, M. Saeys, Effect of boron promotion on the stability of cobalt Fischer–Tropsch catalysts, *J. Catal.* 280 (2011) 50–59, <https://doi.org/10.1016/j.jcat.2011.03.002>.
- [12] J. Xu, L. Chen, K. Tan, A. Borgna, M. Saeys, Effect of boron on the stability of Ni catalysts during steam methane reforming, *J. Catal.* 261 (2009) 158–165, <https://doi.org/10.1016/j.jcat.2008.11.007>.
- [13] A. Fouskas, M. Kollia, A. Kambolis, Ch Papadopoulou, H. Matralis, Boron-modified Ni/Al2O3 catalysts for reduced carbon deposition during dry reforming of methane, *Appl. Catal. A Gen.* 474 (2014) 125–134, <https://doi.org/10.1016/j.apcata.2013.08.016>.
- [14] C. Yuan, L. Zhou, Q. Chen, C. Su, Z. Li, G. Ju, The research on Anti-Nickel contamination mechanism and performance for boron-modified FCC catalyst, *Materials* 15 (2022), <https://doi.org/10.3390/ma15207220>.
- [15] I.I. Shakirov, S.V. Kardashev, S.V. Lysenko, M.P. Boronoev, A.L. Maximov, E. A. Karakhanov, Nickel passivation on cracking catalysts, *Russ. J. Appl. Chem.* 96 (2023) 702–709, <https://doi.org/10.1134/S1070427223060101>.
- [16] I.D. Charisteidis, P.N. Trikalitis, K.S. Triantafyllidis, V. Komvokis, B. Yilmaz, Characterization of Ni-phases and their transformations in fluid catalytic cracking (FCC) catalysts: comparison of conventional versus Boron-based Ni-Passivation, *Catalysts* 13 (2022) 3, <https://doi.org/10.3390/catal13010003>.
- [17] Y. Wang, J. Ma, F. Ren, J. Du, R. Li, Hierarchical architectures of ZSM-5 nanocrystalline aggregates with particular catalysts for lager molecule reaction, *Microporous Mesoporous Mater.* 240 (2017) 22–30, <https://doi.org/10.1016/j.micromeso.2016.10.051>.
- [18] M. Pan, J. Zheng, Y. Liu, W. Ning, H. Tian, R. Li, Construction and practical application of a novel zeolite catalyst for hierarchically cracking of heavy oil, *J. Catal.* 369 (2019) 72–85, <https://doi.org/10.1016/j.jcat.2018.10.032>.
- [19] P. Bai, M. Xie, U.J. Etim, W. Xing, P. Wu, Y. Zhang, B. Liu, Y. Wang, K. Qiao, Z. Yan, Zeolite Y mother liquor modified γ -Al₂O₃ with enhanced Brønsted acidity as active matrix to improve the performance of fluid catalytic cracking catalyst, *Ind. Eng. Chem. Res.* 57 (2018) 1389–1398, <https://doi.org/10.1021/acs.iecr.7b04243>.
- [20] S.I. Zones, A. Benin, S.-J. Hwang, D. Xie, S. Elomari, M.-F. Hsieh, Studies of aluminum reinsertion into borosilicate zeolites with intersecting channels of 10- and 12-ring channel systems, *J. Am. Chem. Soc.* 136 (2014) 1462–1471, <https://doi.org/10.1021/ja4100194>.
- [21] Y. Wang, Y. Bai, P. Chen, Q. Chen, Y. Wang, X. Shu, Synthesis of [B,Al]-EWT-type zeolite and its catalytic Properties, *Molecules* 27 (2022) 5625, <https://doi.org/10.3390/molecules27175625>.
- [22] J.D. Larkin, K.L. Bhat, G.D. Markham, T.D. James, B.R. Brooks, C.W. Bock, A computational characterization of boron–oxygen multiple bonding in HN=CH–CH=CH–NH–BO, *J. Phys. Chem. A* 112 (2008) 8446–8454, <https://doi.org/10.1021/jp800125p>.